



IRWIN AND JOAN JACOBS
CENTER FOR COMMUNICATION AND INFORMATION TECHNOLOGIES

Spatial Frequency Response of Bayer Color Image Formation

Alex Golts and Yoav Y. Schechner

CCIT Report #868
September 2014

■ ■ ■ ■ ■ Electronics
■ ■ ■ ■ ■ Computers
■ ■ ■ ■ ■ Communications

DEPARTMENT OF ELECTRICAL ENGINEERING
TECHNION - ISRAEL INSTITUTE OF TECHNOLOGY, HAIFA 32000, ISRAEL



Spatial Frequency Response of Bayer Color Image Formation

Alex Golts^{1,*} and Yoav Y. Schechner¹

¹*Department of Electrical Engineering, Technion - Israel Inst. of Technology, Haifa 32000, Israel*

compiled: February 25, 2014

Most color imaging systems today are based on a monochrome detector with a color filter array (CFA). Typically the Bayer CFA is used. An imaging system's spatial frequency response (SFR) is one of its most meaningful characteristics. It is directly related to the system's capability to resolve objects. This work presents a model for calculating the SFR of a Bayer color capture system. Our two dimensional model deals with a color input signal, and accounts for both sampling and interpolation processes. It can be applied on any linear interpolation.

OCIS codes: (040.1240) Arrays; (110.0110) Imaging systems; (110.4100) Modulation transfer function.

1. Introduction

The most common color camera technology is based on spatial-multiplexing using a color filter array (CFA): spectral channels are captured in alternating pixels of a single monochrome sensor. A generalized CFA approach has been proposed for hyperspectral imaging [1]. Couillaud et al. applied a frequency domain based method for evaluating the image quality obtained by different CFAs [2]. A Bayer pattern CFA is very common [3]. Following image acquisition, interpolation known as demosaicking is applied, to estimate the color (RGB) values per pixel. Interpolation can be a linear process [4, 5]. Then, each output color pixel can be expressed as a linear function of its surrounding pixels in the raw Bayer sensor image. Thus, it can be expressed as a convolution of the raw Bayer sensor image with some filter kernel. More advanced, non-linear demosaicking methods were introduced more recently [6–8]. While non-linear demosaicking approaches typically result in a sharper image, linear interpolation is still being used. Faster and easier implementation are two main reasons. The notion of spatial frequency response (SFR) is enabled by linear-systems theory. Thus, our Bayer SFR model assumes linear interpolation.

An imaging system's SFR is an important property. It is often used during the system design phase, for comparison between several systems, and in performance prediction models. Such models are required during system design. In some cases, they can be used when the possibility to perform actual experiments is limited due to high risk or cost [9]. For a linear, space-invariant system, the SFR is given by the system's modulation transfer function (MTF). A thermal imaging system's minimum resolvable temperature difference (MRTD) [10] is

an important performance measure. It is spatial frequency dependant, and is inversely proportional to the MTF. The same is true for minimum resolvable contrast (MRC) [11], an analog of the MRTD in visible light systems.

Dubois [12] analyzed the SFR of a raw Bayer signal, excluding interpolation. On the other hand, Elor et al. [13] analyzed the SFR of linear interpolation of Bayer-based data, excluding the raw acquisition SFR. The scene in [13] is assumed to be monochrome. Ref. [13] also assumed signal integration along the vertical axis. This assumption simplified the mathematical derivations, resulting in a one-dimensional SFR. However, vertical integration does not take place in practice. We show that there actually is a frequency response in both directions. Interestingly, this is the case even if the input signal varies only in the horizontal direction. Hubel et al. [14] presented empirical measurements of the SFR of a Bayer sensor, and compared them to a FOVEON X3 sensor, for which limitations peculiar to a CFA do not exist.

In this work, we present a unified model. We analyze the *two-dimensional* SFR of a Bayer imaging system, caused by *both* CFA sampling and linear interpolation processes. Moreover, we do not limit the analysis to a monochrome scene. In contrast to Refs. [12, 13], we present a simulation which is consistent with our theoretical model for Bayer SFR.

2. Background

2.A. Bayer image formation

The Bayer image formation process is illustrated in Fig. 1. A Bayer CFA [3] is illustrated in the middle. Let x and y denote discrete horizontal and vertical axes, respectively. We define their origin to be at the bottom left point of the Bayer grid which is illustrated in Fig. 1. An RGB signal is denoted by $s_R(x, y)$, $s_G(x, y)$ and $s_B(x, y)$. These are the original signals that the Bayer system aims to estimate, while using a single

* Corresponding author: alexgo@tx.technion.ac.il

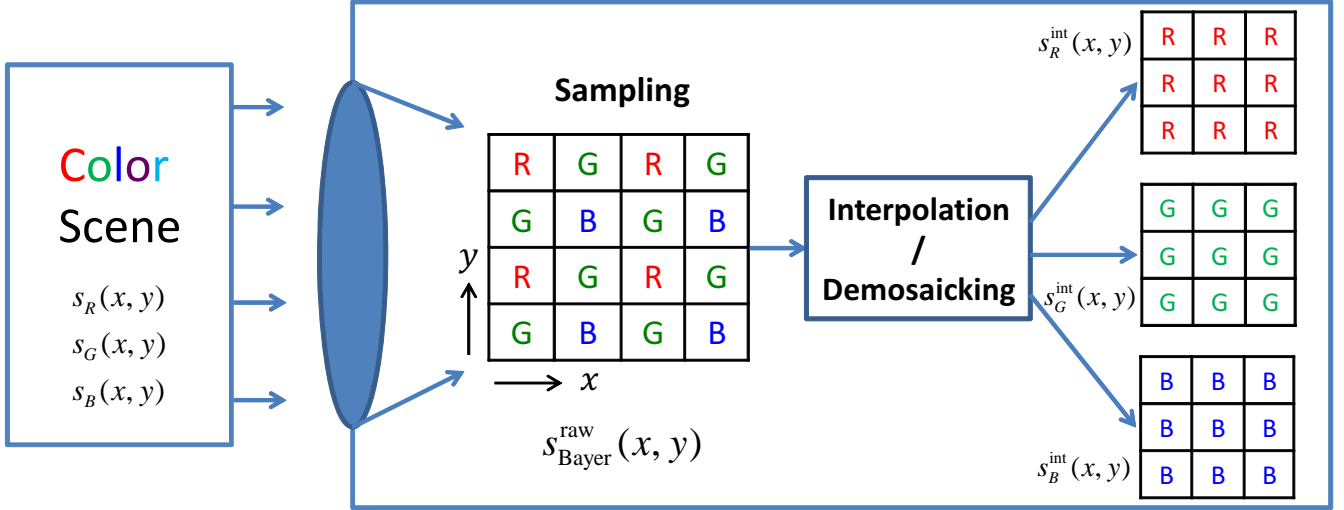


Fig. 1. Bayer image formation process.

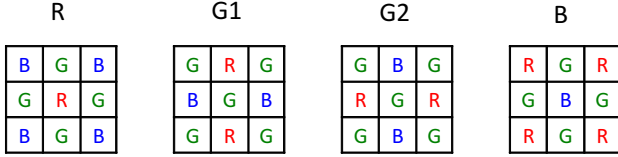


Fig. 2. Four pixel types in the Bayer CFA. Each pixel type is shown in the middle, with eight nearest neighbors.

monochrome detector. These signals are sampled by a Bayer CFA. Let $s_{\text{Bayer}}^{\text{raw}}(x, y)$ be the raw signal sampled by the Bayer sensor. Subsequent interpolation yields three images $s_R^{\text{int}}(x, y)$, $s_G^{\text{int}}(x, y)$ and $s_B^{\text{int}}(x, y)$, corresponding to the R, G and B color channels. These are the estimates of the original, unsampled signals.

A Bayer CFA sensor [3] consists of four pixel types [13]. These types are distinguished by their neighborhood (See Fig. 2). The raw Bayer signal, $s_{\text{Bayer}}^{\text{raw}}(x, y)$, is

$$s_{\text{Bayer}}^{\text{raw}}(x, y) = \begin{cases} s_R(x, y) & \text{for "R" type } (x, y) \\ s_G(x, y) & \text{for "G1" type } (x, y) \\ s_G(x, y) & \text{for "G2" type } (x, y) \\ s_B(x, y) & \text{for "B" type } (x, y) \end{cases} \quad (1)$$

A general linear interpolation process can be expressed as follows. Each of the four pixel types has three impulse response kernels, which correspond to resulting interpolated R, G, B signals. We denote these kernels h_c^t , where $c \in [R, G, B]$ and $t \in [R, G1, G2, B]$. As an example, for bilinear interpolation [5], h_c^t are given [13] in Fig. 3

Then, we can write $s_c^{\text{int}}(x)$, the Bayer RGB channels

after interpolation,

$$s_c^{\text{int}}(x, y) = \begin{cases} s_{\text{Bayer}}^{\text{raw}} * h_c^R & \text{for "R" type } (x, y) \\ s_{\text{Bayer}}^{\text{raw}} * h_c^{G1} & \text{for "G1" type } (x, y) \\ s_{\text{Bayer}}^{\text{raw}} * h_c^{G2} & \text{for "G2" type } (x, y) \\ s_{\text{Bayer}}^{\text{raw}} * h_c^B & \text{for "B" type } (x, y) \end{cases}, \quad (2)$$

where $*$ denotes 2D discrete convolution.

2.B. Extension of MTF

Ref. [13] extends the definition of MTF to include linear systems which are space-variant. Such system is a Bayer CFA sensor followed by linear interpolation. Consider $s_{\text{in}}(x, y)$ and $s_{\text{out}}(x, y)$ to respectively be the input and output signals of a Bayer system. Let $S_{\text{in}}(u, v)$ and $S_{\text{out}}(u, v)$ be the 2D Discrete-Time Fourier Transform (2D-DTFT) of $s_{\text{in}}(x, y)$ and $s_{\text{out}}(x, y)$, respectively. A spatial frequency (u, v) has units of [cy/pixel]. This is the convention we use throughout the paper, thus from here on, units shall be omitted. We define a *variant MTF* (VMTF) at a spatial frequency $(u, v) = (u', v')$ as

$$\text{VMTF}(u', v') \equiv \left| \frac{S_{\text{out}}(u', v')}{S_{\text{in}}(u', v')} \right|. \quad (3)$$

Consider an input signal with a single spatial frequency (u', v') . For a linear, space-invariant system, an output signal only contains the same spatial frequency. Thus, for such a system, the above definition degenerates to the standard definition for MTF: the attenuation at each frequency component.

3. SFR of a Bayer color sensor

In this section, we obtain the SFR corresponding to Bayer sampling and linear interpolation. We then combine these two processes to obtain the total SFR of a Bayer-based, color imaging system.

$$\begin{aligned}
h_R^R &= \begin{pmatrix} 0 & 0 & 0 \\ 0 & 1 & 0 \\ 0 & 0 & 0 \end{pmatrix} & h_R^{G1} &= \begin{pmatrix} 0 & 0.5 & 0 \\ 0 & 0 & 0 \\ 0 & 0.5 & 0 \end{pmatrix} & h_R^{G2} &= \begin{pmatrix} 0 & 0 & 0 \\ 0.5 & 0 & 0.5 \\ 0 & 0 & 0 \end{pmatrix} & h_R^B &= \begin{pmatrix} 0.25 & 0 & 0.25 \\ 0 & 0 & 0 \\ 0.25 & 0 & 0.25 \end{pmatrix} \\
h_G^R &= \begin{pmatrix} 0 & 0.25 & 0 \\ 0.25 & 0 & 0.25 \\ 0 & 0.25 & 0 \end{pmatrix} & h_G^{G1} &= \begin{pmatrix} 0 & 0 & 0 \\ 0 & 1 & 0 \\ 0 & 0 & 0 \end{pmatrix} & h_G^{G2} &= \begin{pmatrix} 0 & 0 & 0 \\ 0 & 1 & 0 \\ 0 & 0 & 0 \end{pmatrix} & h_G^B &= \begin{pmatrix} 0 & 0.25 & 0 \\ 0.25 & 0 & 0.25 \\ 0 & 0.25 & 0 \end{pmatrix} \\
h_B^R &= \begin{pmatrix} 0.25 & 0 & 0.25 \\ 0 & 0 & 0 \\ 0.25 & 0 & 0.25 \end{pmatrix} & h_B^{G1} &= \begin{pmatrix} 0 & 0 & 0 \\ 0.5 & 0 & 0.5 \\ 0 & 0 & 0 \end{pmatrix} & h_B^{G2} &= \begin{pmatrix} 0 & 0.5 & 0 \\ 0 & 0 & 0 \\ 0 & 0.5 & 0 \end{pmatrix} & h_B^B &= \begin{pmatrix} 0 & 0 & 0 \\ 0 & 1 & 0 \\ 0 & 0 & 0 \end{pmatrix}
\end{aligned}$$

Fig. 3. The kernels h_c^t , corresponding to bilinear interpolation.

3.A. Bayer sampling SFR

Define the following notation, for a general 2D frequency domain signal $U(u, v)$

$$\begin{aligned}
\tilde{U} &\equiv U(u, v) \\
\tilde{U}^\uparrow &\equiv U\left(u, v - \frac{1}{2}\right) \\
\tilde{U}^{\rightarrow} &\equiv U\left(u - \frac{1}{2}, v\right) \\
\tilde{U}^{\nearrow} &\equiv U\left(u - \frac{1}{2}, v - \frac{1}{2}\right).
\end{aligned} \tag{4}$$

We use this notation for convenience, from here on. As shown in App. A, the DTFT of Eq. (1) is

$$\begin{aligned}
S_{\text{Bayer}}^{\text{raw}}(u, v) &= \frac{1}{4} [\tilde{S}_R + 2\tilde{S}_G + \tilde{S}_B] + \frac{1}{4} [\tilde{S}_B^\uparrow - \tilde{S}_R^\uparrow] + \\
&\frac{1}{4} [\tilde{S}_B^{\rightarrow} - \tilde{S}_R^{\rightarrow}] + \frac{1}{4} [\tilde{S}_R^{\nearrow} - 2\tilde{S}_G^{\nearrow} + \tilde{S}_B^{\nearrow}].
\end{aligned} \tag{5}$$

Fig. 4 is a visual representation of Eq. (5).

Following traditional linear-systems analysis, we wish to find the response of the Bayer system to a single frequency input. Consider an input signal that varies in the horizontal direction at a spatial frequency $u' \in [0, \frac{1}{2}]$. The spatial frequency in the vertical direction is $v' = 0$. Thus, the signal is given by

$$s_c(x, y) = A_c \cos(2\pi u' x + \varphi_c), \tag{6}$$

where $c \in [R, G, B]$, A_c is the signal amplitude, and φ_c represents a per-color phase component. A background, or ‘‘DC’’ component B_c can be present. It does not change by Bayer image formation, assuming an energy-preserving interpolation. Thus, we ignore it in our analysis.

Let $A_c = 2$. Fig. 5a shows the modulus of $S_c(u, v)$, the DTFT of $s_c(x, y)$, in the first quadrant of the frequency domain. It is simply a delta function with unit height.

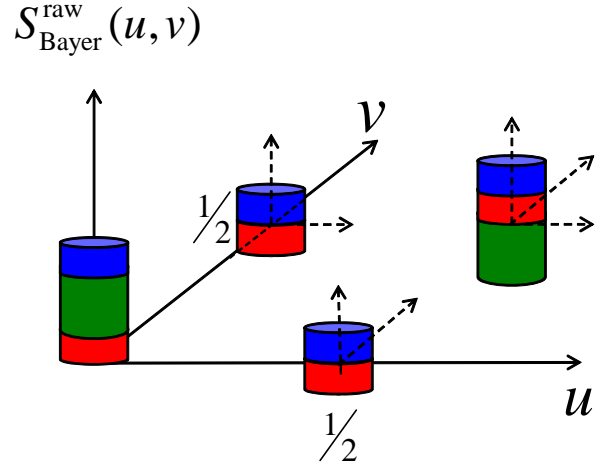


Fig. 4. A visual representation of $S_{\text{Bayer}}^{\text{raw}}(u, v)$, according to Eq. (5). It shows the first quadrant of the frequency domain. A cylinder centered about some spatial frequency, represents a signal replica centered about that frequency. The colored slices represent the relative contribution of the corresponding RGB components at each signal replica.

Using the DTFT of Eq. (6) in Eq. (5) yields

$$\begin{aligned}
S_{\text{Bayer}}^{\text{raw}}(u, v) &= \tilde{S}_c \text{VMTF}_c^{\text{samp}} + \tilde{S}_c^\uparrow \text{SR}_{c,\uparrow}^{\text{samp}} + \\
&\tilde{S}_c^{\rightarrow} \text{SR}_{c,\rightarrow}^{\text{samp}} + \tilde{S}_c^{\nearrow} \text{SR}_{c,\nearrow}^{\text{samp}},
\end{aligned} \tag{7}$$

where

$$\text{VMTF}_c^{\text{samp}} \equiv \frac{A_R e^{i2\pi\varphi_R} + 2A_G e^{i2\pi\varphi_G} + A_B e^{i2\pi\varphi_B}}{4A_c e^{i2\pi\varphi_c}}. \tag{8}$$

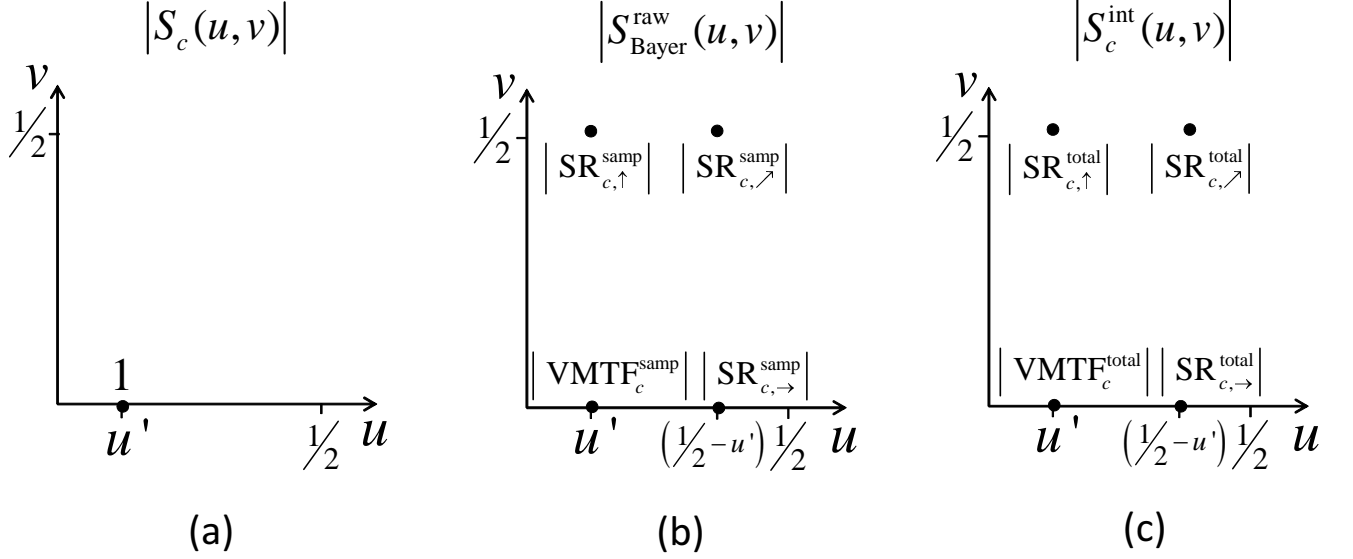


Fig. 5. Schematic view of $|S_c(u, v)|$, $|S_{\text{Bayer}}^{\text{raw}}(u, v)|$ and $|S_c^{\text{int}}(u, v)|$. The delta function corresponding to the original signal $s_c(x, y)$ is reproduced at three spatial frequencies, in addition to the original signal frequency. The ratios of $S_{\text{Bayer}}^{\text{raw}}(u, v)$ to $S_c(u', v')$ in each frequency are given in Eqs. (8,9). The ratios of $S_c^{\text{int}}(u, v)$ to $S_c(u, v)$ in each frequency are given in Eqs. (14,15). In (b), note that $|SR_{c,\uparrow}^{\text{samp}}|$, and $|SR_{c,\nearrow}^{\text{samp}}|$ appear in the first quadrant of the Fourier domain, although according to Eq. 7, they correspond to larger frequencies. This stems from the symmetric property of the Fourier transform. In (c), the same holds for $|SR_{c,\rightarrow}^{\text{total}}|$, and $|SR_{c,\nearrow}^{\text{total}}|$.

and

$$\begin{aligned} SR_{c,\uparrow}^{\text{samp}} &\equiv \frac{A_B e^{i2\pi\varphi_B} - A_R e^{i2\pi\varphi_R}}{4A_c e^{i2\pi\varphi_c}} \\ SR_{c,\rightarrow}^{\text{samp}} &\equiv \frac{A_B e^{i2\pi\varphi_B} - A_R e^{i2\pi\varphi_R}}{4A_c e^{i2\pi\varphi_c}} \\ SR_{c,\nearrow}^{\text{samp}} &\equiv \frac{A_R e^{i2\pi\varphi_R} - 2A_G e^{i2\pi\varphi_G} + A_B e^{i2\pi\varphi_B}}{4A_c e^{i2\pi\varphi_c}}. \end{aligned} \quad (9)$$

Eq. (8) defines the VMTF of each color due to spatial sampling, following the definition in Eq. (3). Here, $S_c(u, v)$ represents the input signal, and $S_{\text{Bayer}}^{\text{raw}}(u, v)$ is the output. It represents attenuation of a frequency component (u, v) , due to Bayer sampling. The terms in Eq. (9) represent “parasitic” responses in spatial frequencies other than the input frequency. These terms stem from the space-variance of the system. In [13], analysis was reduced to one dimension, and integration in the vertical direction was assumed. Under these assumptions, only one “parasitic” term is obtained due to Bayer interpolation. It was referred to as *spurious response* (SR), and we use this terminology. We see that three SR terms are generally obtained due to Bayer sampling of a color input signal. They involve both horizontal and vertical “parasitic” frequencies.

Fig. 5b shows the modulus of $S_{\text{Bayer}}^{\text{raw}}(u, v)$, the DTFT of $s_{\text{Bayer}}^{\text{raw}}(x, y)$, in the first quadrant of the frequency domain.

To gain a better intuition of these results, we illustrate two examples. Assume $\varphi_c = 0$, $\forall c$ (we discuss this

assumption later on, in Sec. 4.A). As a first example, let $\{A_c\} = [1, 1, 1]$, representing a gray signal. Fig. 6a shows a visualization of $S_{\text{Bayer}}^{\text{raw}}(u, v)$. In this case, all SR terms are null. This case is analyzed in Ref. [13], which assumes a colorless input. Sampling causes no spurious response in this case. In a second example, $\{A_c\} = [3, 1, 1]$, representing a reddish signal. Fig. 6b visualizes $S_{\text{Bayer}}^{\text{raw}}(u, v)$ in that case.

3.B. Bayer linear interpolation SFR

We now wish to account for the VMTF and SR corresponding to Bayer linear interpolation.

Let $H_c^t(u, v)$ be the DTFT of a kernel $h_c^t(x, y)$ (see Sec. 2.A). As shown in App. A (using the notation in Eq. 4), the DTFT of Eq. (2) is

$$\begin{aligned} S_c^{\text{int}}(u, v) &= \tilde{S}_{\text{Bayer}}^{\text{raw}} \text{VMTF}_c^{\text{int}} + \tilde{S}_{\text{Bayer}}^{\text{raw}\uparrow} \text{SR}_{c,\uparrow}^{\text{int}} + \\ &\tilde{S}_{\text{Bayer}}^{\text{raw}\rightarrow} \text{SR}_{c,\rightarrow}^{\text{int}} + \tilde{S}_{\text{Bayer}}^{\text{raw}\nearrow} \text{SR}_{c,\nearrow}^{\text{int}}, \end{aligned} \quad (10)$$

where

$$\text{VMTF}_c^{\text{int}} \equiv \frac{1}{4} \left[\tilde{H}_c^R + \tilde{H}_c^{G1} + \tilde{H}_c^{G2} + \tilde{H}_c^B \right], \quad (11)$$

and

$$\begin{aligned} \text{SR}_{c,\uparrow}^{\text{int}} &\equiv \frac{1}{4} \left[-\tilde{H}_c^{R\uparrow} + \tilde{H}_c^{G1\uparrow} - \tilde{H}_c^{G2\uparrow} + \tilde{H}_c^{B\uparrow} \right] \\ \text{SR}_{c,\rightarrow}^{\text{int}} &\equiv \frac{1}{4} \left[-\tilde{H}_c^{R\rightarrow} - \tilde{H}_c^{G1\rightarrow} + \tilde{H}_c^{G2\rightarrow} + \tilde{H}_c^{B\rightarrow} \right] \\ \text{SR}_{c,\nearrow}^{\text{int}} &\equiv \frac{1}{4} \left[\tilde{H}_c^{R\nearrow} - \tilde{H}_c^{G1\nearrow} - \tilde{H}_c^{G2\nearrow} + \tilde{H}_c^{B\nearrow} \right]. \end{aligned} \quad (12)$$

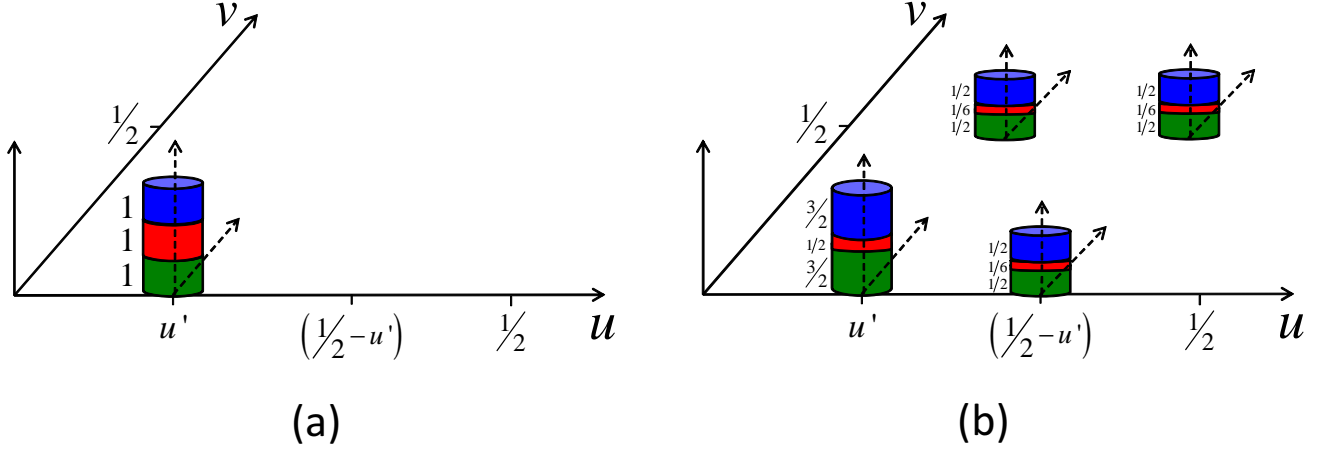


Fig. 6. A visualization of $S_{\text{Bayer}}^{\text{raw}}(u, v)$ (while $\varphi_c = 0 \ \forall c$). Each cylinder represents a VMTF or SR term. The colored slices represent the relative contribution of the corresponding RGB components to each term. The value of each component appears to its left. Two examples are shown: a) A gray signal. b) A reddish signal.

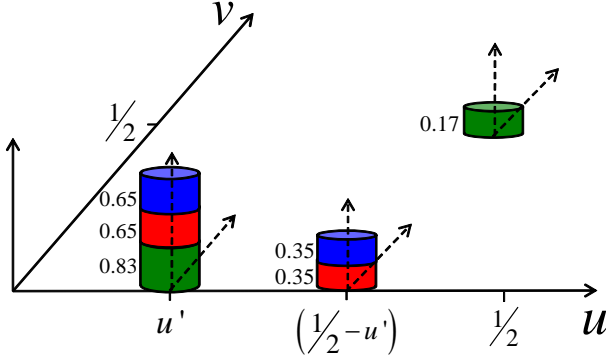


Fig. 7. A visualization of $S_c^{\text{int}}(u, v)$ given $(u', v') = (0.2, 0)$ and bilinear interpolation. Each cylinder represents a VMTF or SR term. The colors represent the relative contribution of the corresponding RGB components to each term.

Eq. (11) defines the VMTF which corresponds to Bayer linear interpolation, for each color channel, following the definition in Eq. (3). Here, $S_{\text{Bayer}}^{\text{raw}}(u, v)$ represents the input signal, and $S_c^{\text{int}}(u, v)$ is the output. The terms in Eq. (12) are the SR terms created by the interpolation process.

As an example, let $(u', v') = (0.2, 0)$, and assume bilinear interpolation (see Fig. 3). Fig. 7 shows a visualization of $S_c^{\text{int}}(u, v)$. As seen from Eqs. (11,12), the VMTF and SR terms which correspond to Bayer interpolation, are independent of $\{A_c\}$ and $\{\varphi_c\}$. They depend solely on the signal's spatial frequency, and the interpolation kernels.

3.C. Total Bayer SFR

As shown in App. B, using Eq. (7) in Eq. (10), yields

$$S_c^{\text{int}}(u, v) = \tilde{S}_c \text{VMTF}_c^{\text{total}} + \tilde{S}_c^{\uparrow} \text{SR}_{c,\uparrow}^{\text{total}} + \tilde{S}_c^{\rightarrow} \text{SR}_{c,\rightarrow}^{\text{total}} + \tilde{S}_c^{\nearrow} \text{SR}_{c,\nearrow}^{\text{total}}, \quad (13)$$

where

$$\begin{aligned} \text{VMTF}_c^{\text{total}} \equiv & \left[\text{VMTF}_c^{\text{samp}} \text{VMTF}_c^{\text{int}} + \text{SR}_{c,\uparrow}^{\text{samp}} \text{SR}_{c,\uparrow}^{\text{int}} + \right. \\ & \left. \text{SR}_{c,\rightarrow}^{\text{samp}} \text{SR}_{c,\rightarrow}^{\text{int}} + \text{SR}_{c,\nearrow}^{\text{samp}} \text{SR}_{c,\nearrow}^{\text{int}} \right]. \end{aligned} \quad (14)$$

and

$$\begin{aligned} \text{SR}_{c,\uparrow}^{\text{total}} \equiv & \left[\text{SR}_{c,\uparrow}^{\text{samp}} \text{VMTF}_c^{\text{int}} + \text{VMTF}_c^{\text{samp}} \text{SR}_{c,\uparrow}^{\text{int}} + \right. \\ & \left. \text{SR}_{c,\nearrow}^{\text{samp}} \text{SR}_{c,\rightarrow}^{\text{int}} + \text{SR}_{c,\rightarrow}^{\text{samp}} \text{SR}_{c,\nearrow}^{\text{int}} \right] \\ \text{SR}_{c,\rightarrow}^{\text{total}} \equiv & \left[\text{SR}_{c,\rightarrow}^{\text{samp}} \text{VMTF}_c^{\text{int}} + \text{VMTF}_c^{\text{samp}} \text{SR}_{c,\rightarrow}^{\text{int}} + \right. \\ & \left. \text{SR}_{c,\nearrow}^{\text{samp}} \text{SR}_{c,\uparrow}^{\text{int}} + \text{SR}_{c,\uparrow}^{\text{samp}} \text{SR}_{c,\nearrow}^{\text{int}} \right] \\ \text{SR}_{c,\nearrow}^{\text{total}} \equiv & \left[\text{SR}_{c,\nearrow}^{\text{samp}} \text{VMTF}_c^{\text{int}} + \text{SR}_{c,\rightarrow}^{\text{samp}} \text{SR}_{c,\uparrow}^{\text{int}} + \right. \\ & \left. \text{SR}_{c,\uparrow}^{\text{samp}} \text{SR}_{c,\rightarrow}^{\text{int}} + \text{VMTF}_c^{\text{samp}} \text{SR}_{c,\nearrow}^{\text{int}} \right]. \end{aligned} \quad (15)$$

Fig. 5c shows the modulus of $S_c^{\text{int}}(u, v)$, the DTFT of $s_c^{\text{int}}(x, y)$, in the first quadrant of the frequency domain.

Eq. (14) defines the total VMTF which accounts for the Bayer imaging formation (sampling and interpolation), for each color channel, following the definition in

Eq. (3). Here, $S_c(u, v)$ represents the input signal, and $S_c^{\text{int}}(u, v)$ is the output. The terms in Eq. (15) are the total SR terms of the Bayer system.

4. Simulation

4.A. Identical phase approximation

In the following, we reach an assumption about natural images. We then use it in our simulation.

Objects typically have a similar structure in all color channels. Therefore, can we approximate the phases $\{\varphi_c\}$ to be similar? We studied this question using natural RGB images.

Let I_R , I_G and I_B be red, green and blue image components. Let \mathbf{F} be the discrete Fourier transform (DFT). We apply DFT on each color channel independently

$$\begin{aligned} \mathbf{F}\{I_R\} &\equiv |\mathbf{F}\{I_R\}| \exp(j\angle\mathbf{F}\{I_R\}) \\ \mathbf{F}\{I_G\} &\equiv |\mathbf{F}\{I_G\}| \exp(j\angle\mathbf{F}\{I_G\}) \\ \mathbf{F}\{I_B\} &\equiv |\mathbf{F}\{I_B\}| \exp(j\angle\mathbf{F}\{I_B\}) . \end{aligned} \quad (16)$$

Here $|\cdot|$ denotes the magnitude of each spatial frequency component and \angle denotes the phase per frequency. We define the following distance measures for the absolute phase differences

$$\begin{aligned} \tilde{\mathbf{d}}_{\angle(R-G)} &= |\angle\mathbf{F}\{I_R\} - \angle\mathbf{F}\{I_G\}| \\ \tilde{\mathbf{d}}_{\angle(R-B)} &= |\angle\mathbf{F}\{I_R\} - \angle\mathbf{F}\{I_B\}| \\ \tilde{\mathbf{d}}_{\angle(G-B)} &= |\angle\mathbf{F}\{I_G\} - \angle\mathbf{F}\{I_B\}| . \end{aligned} \quad (17)$$

The distance measures should take values between 0° and 180° . Hence, we define the following

$$\begin{aligned} \mathbf{d}_{\angle(R-G)} &= \min(\tilde{\mathbf{d}}_{\angle(R-G)} , 360^\circ - \tilde{\mathbf{d}}_{\angle(R-G)}) \\ \mathbf{d}_{\angle(R-B)} &= \min(\tilde{\mathbf{d}}_{\angle(R-B)} , 360^\circ - \tilde{\mathbf{d}}_{\angle(R-B)}) \\ \mathbf{d}_{\angle(G-B)} &= \min(\tilde{\mathbf{d}}_{\angle(G-B)} , 360^\circ - \tilde{\mathbf{d}}_{\angle(G-B)}) . \end{aligned} \quad (18)$$

Note that $\tilde{\mathbf{d}} \equiv 360^\circ - \mathbf{d}$, due to the periodicity of Fourier phase components. Fig. 8 shows the histograms of $\mathbf{d}_{\angle(R-G)}$, $\mathbf{d}_{\angle(R-B)}$ and $\mathbf{d}_{\angle(G-B)}$, based on 963 natural images taken from [15]. All histograms peak at 0° .

As a particular example, Fig. 9a shows one image of a fighter aircraft over a sky background. Fig. 10 shows the sum of histograms of $\mathbf{d}_{\angle(R-G)}$, $\mathbf{d}_{\angle(R-B)}$ and $\mathbf{d}_{\angle(G-B)}$, for that image. Fig. 9b shows the original image, after replacing each color component's Fourier phase, with another component's phase, at random

$$\begin{aligned} \angle\mathbf{F}_{(k,l)}^{\text{new}}\{I_R\} &= \begin{cases} \angle\mathbf{F}_{(k,l)}\{I_G\} & \text{with probability } 0.5 \\ \angle\mathbf{F}_{(k,l)}\{I_B\} & \text{with probability } 0.5 \end{cases} \\ \angle\mathbf{F}_{(k,l)}^{\text{new}}\{I_G\} &= \begin{cases} \angle\mathbf{F}_{(k,l)}\{I_R\} & \text{with probability } 0.5 \\ \angle\mathbf{F}_{(k,l)}\{I_B\} & \text{with probability } 0.5 \end{cases} \\ \angle\mathbf{F}_{(k,l)}^{\text{new}}\{I_B\} &= \begin{cases} \angle\mathbf{F}_{(k,l)}\{I_R\} & \text{with probability } 0.5 \\ \angle\mathbf{F}_{(k,l)}\{I_G\} & \text{with probability } 0.5 \end{cases} , \end{aligned} \quad (19)$$

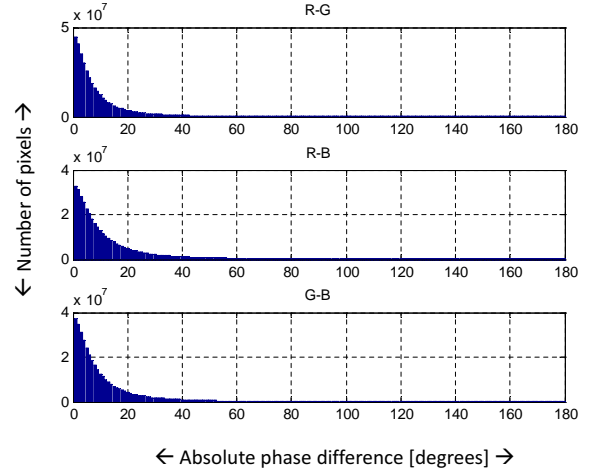


Fig. 8. Histograms of the absolute phase differences between the color channels, for 963 natural images.



Fig. 9. a) Original RGB image of a fighter aircraft over sky background. b) The image, after replacing each color component's Fourier phase with another color's phase component.

where (k, l) are the 2D DFT frequency indices. It is evident from Fig. 9b that such deliberate disturbance retains much of the original structure. Hence, we believe that assuming identical phase for all the image channels is a reasonable working assumption. Consequently, we may drop the phases $\{\varphi_c\}$ from our analysis. The RGB signal equation (Eq. 6) degenerates to

$$s_c(x, y) \approx A_c \cos(2\pi u'x) \quad \forall c . \quad (20)$$

In the following, we use this approximation.

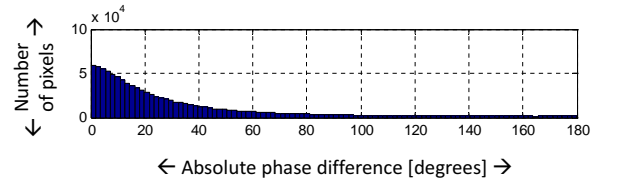


Fig. 10. Sum of the histograms of the absolute phase differences between color channels of Fig. 9a.

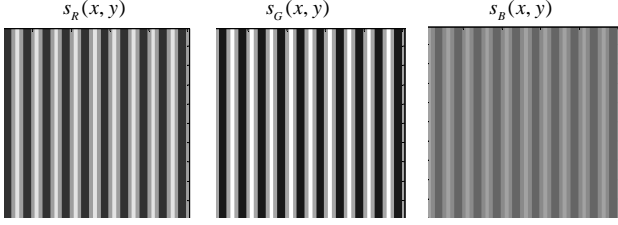


Fig. 11. An RGB signal, $s_c(x, y)$.

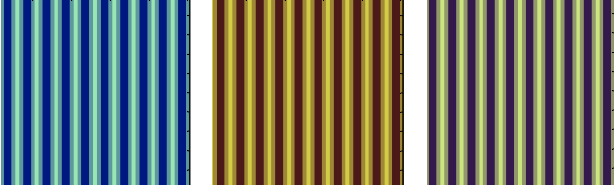


Fig. 12. Three possible RGB color representations for $\mathbf{s}(x, y)$.

4.B. Bayer image formation simulation

This section simulates Bayer image formation. It demonstrates the effect of sampling and linear demosaicking, in both spatial and frequency domains. The simulation sets $\{A_c\} = [15, 20, 5]$, input spatial frequency $(u', v') = (0.2, 0)$ (modulation only in the horizontal direction), and bilinear interpolation (Fig. 3). It also neglects $\{\varphi_c\}$, following Sec. 4.A. Fig. 11 shows the input, $s_c(x, y)$, for each $c \in [R, G, B]$ separately. An RGB color image is also affected by the three RGB background values, and overall normalization (to bound each channel between values of 0 and 1). Fig. 12 shows three examples of RGB color representations for $\mathbf{s}(x, y)$, in our example. Fig. 13 shows the raw Bayer signal, $s_{\text{Bayer}}^{\text{raw}}(x, y)$ from Eq. (1), and its DTFT, $S_{\text{Bayer}}^{\text{raw}}(u, v)$, from Eq. (7).

Fig. 14 shows the signals after Bayer interpolation, $s_c^{\text{int}}(x, y)$, from Eq. (2), and their DTFT, $S_c^{\text{int}}(u, v)$, from Eq. (10). Fig. 15 shows the color representations of $\mathbf{s}^{\text{int}}(x, y)$, which correspond to background RGB values as in Fig. 12. The simulated peak values of $S_{\text{Bayer}}^{\text{raw}}(u, v)$ and $S_c^{\text{int}}(u, v)$, all agree well with their analytic expressions (Eqs. 8, 9, 14, 15). The simulated and theoretical values are shown in Fig. 16, along with a relative error measure. A small relative error is caused by numerical inaccuracies of the simulation. A part of them is due to the fact that the simulation computed 2D-DFT (over large images, resembling large focal plane array detectors available today), rather than 2D-DTFT, which assumes 2D signals of infinite length.

5. Discussion

We analyzed the SFR of Bayer CFA imaging systems. Our model for SFR accounts for both Bayer color signal sampling, and linear interpolation processes, in two

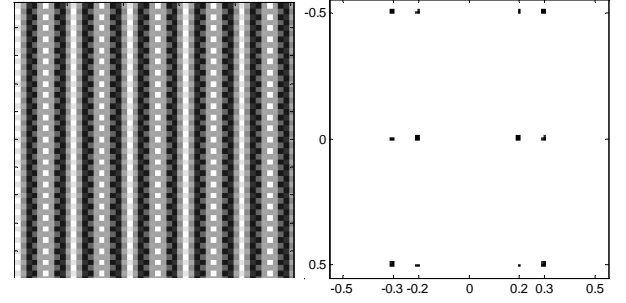


Fig. 13. [left] $s_{\text{Bayer}}^{\text{raw}}(x, y)$. [right] $S_{\text{Bayer}}^{\text{raw}}(u, v)$. Note the dominant horizontal modulation which can be observed in the spatial domain. It corresponds to the input spatial frequency $u' = 0.2$. The “parasitic” high-frequency modulation in both horizontal and vertical directions is represented by the SR terms due to sampling (Eq. 9). These terms are clearly seen in the frequency domain.

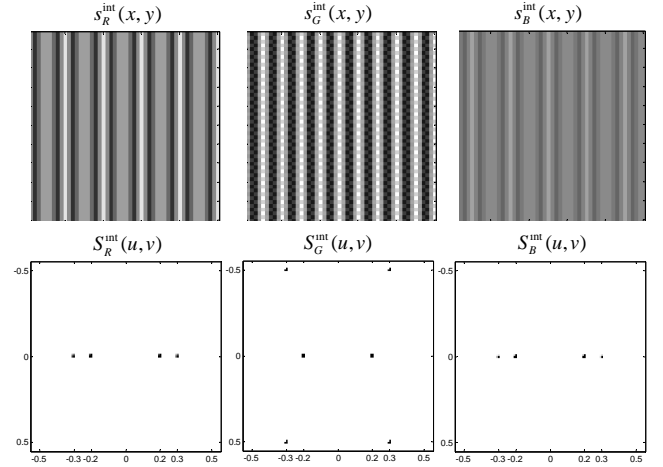


Fig. 14. Signal after interpolation, $s_c^{\text{int}}(x, y)$, and their DTFT, $S_c^{\text{int}}(u, v)$.

dimensions. We showed that the SFR of a Bayer sensor consists of a VMTF, a generalization of the well known MTF function to the case of space-variant systems. Similarly to the MTF, the VMTF represents the system’s signal attenuation at a spatial frequency identical to the input signal frequency. Unlike linear, space-invariant systems, in the Bayer sensor, there are also SR terms, which represent a parasitic contribution in spatial frequencies other than the input signal’s frequency. This parasitic modulation occurs in both the horizontal and vertical direction, even if the input signal is purely horizontal. We present analytical formulae to the VMTF and SR terms of a Bayer sensor, and a numerical simulation which confirms the theoretical derivation.

In future work, new linear interpolation (demosaicking) algorithms can be suggested, based on our SFR model. Interpolation kernels can be optimized in order to achieve a desired frequency response. A similar

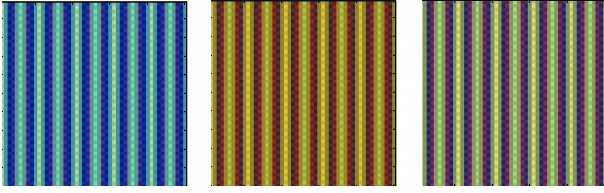


Fig. 15. Three possible RGB color representations for $s^{\text{int}}(x, y)$. Note the difference from the original signals $s(x, y)$, shown in Fig. 12. Parasitic modulation in both the horizontal and vertical directions exists in $s^{\text{int}}(x, y)$. The SR terms (Eq. 15) express this artifact.

	Simulation			Theoretical			Error [%]		
	R	G	B	R	G	B	R	G	B
VMTF ^{samp}	1.001	0.751	3.004	1	0.75	3	0.1	0.13	0.13
SR _→ ^{samp}	0.165	0.124	0.496	0.167	0.125	0.5	1.2	0.8	0.8
SR _↑ ^{samp}	0.168	0.126	0.505	0.167	0.125	0.5	0.6	0.8	1
SR _↗ ^{samp}	0.330	0.247	0.989	0.333	0.25	1	0.9	1.2	1.1
VMTF ^{total}	0.655	0.828	0.672	0.655	0.827	0.655	0	0.12	2.6
SR _→ ^{total}	0.338	0.005	0.346	0.346	0	0.346	2.31	---	0
SR _↑ ^{total}	0	0.002	0	0	0	0	---	---	---
SR _↗ ^{total}	0	0.171	0	0	0.173	0	---	1.16	---

Fig. 16. Simulated and theoretical peaks in the SFR, and the relative simulation error.

approach of frequency domain analysis may be applied in order to design CFAs other than Bayer. Depending on a system's frequency response requirements and constraints, more suitable CFA designs can perhaps be achieved. It is also worth considering a unified design of a CFA with corresponding interpolation kernels. This may lead to improved overall performance. In addition, our work can serve as a basis to analyzing the resolution limits in Bayer imaging sensors. Such analysis can be helpful in Bayer imaging systems design, performance evaluation, and in comparison between different systems.

6. Acknowledgements

The work was supported in part by the Israel Science Foundation (Grant 1467/12) and the VPR Fund of the Technion. This work was conducted in the Ollendorff Minerva Center. Minerva is funded through the BMBF.

Appendix A: Proof of Eqs. (5,10)

Properties of the DTFT in 1D settings (see Ref. [16]) are extended to the 2D case. We then use these properties to prove Eqs. (5,10).

1. Downsampling

Let $\mathbf{D}_{(a,b)}$ ($a, b \subseteq \mathbb{N}$) denote a downsampling operator. A discrete 2D signal $g(x, y)$ is a downsampling of $f(x, y)$

when

$$g(x, y) \equiv \mathbf{D}_{(a,b)}f(x, y) = f(ax, by) . \quad (\text{A1})$$

The DTFT of Eq. (A1) is

$$G(u, v) = \frac{1}{ab} \sum_{p=0}^{a-1} \sum_{q=0}^{b-1} F\left(\frac{u-p}{a}, \frac{v-q}{b}\right) , \quad (\text{A2})$$

where $F(u, v)$ is the DTFT of $f(x, y)$.

2. Upsampling

Let $\mathbf{U}_{(a,b)}$ ($a, b \subseteq \mathbb{N}$) denote an upsampling operator. A discrete 2D signal $g(x, y)$ is an upsampling of $f(x, y)$ when

$$g(x, y) \equiv \mathbf{U}_{(a,b)}f(x, y) = \begin{cases} f\left(\frac{x}{a}, \frac{y}{b}\right) & \text{for } \frac{x}{a}, \frac{y}{b} \subseteq \mathbb{Z}, \\ 0 & \text{otherwise.} \end{cases} \quad (\text{A3})$$

The DTFT of Eq. (A3) is

$$G(u, v) = F(au, bv) . \quad (\text{A4})$$

3. Translation

Let $\mathbf{T}_{(a,b)}$ ($a, b \subseteq \mathbb{N}$) denote a translation operator. A discrete 2D signal $g(x, y)$ is a translation of $f(x, y)$ when

$$g(x, y) \equiv \mathbf{T}_{(a,b)}f(x, y) = f(x-a, y-b) . \quad (\text{A5})$$

The DTFT of Eq. (A5) is

$$G(u, v) = e^{-i2\pi(ua+vb)}F(u, v) . \quad (\text{A6})$$

4. Proof

Let

$$g(x, y) = \begin{cases} f_R(x, y) & \text{for odd } x, \text{ odd } y \text{ ("R" type)} \\ f_{G1}(x, y) & \text{for odd } x, \text{ even } y \text{ ("G1" type)} \\ f_{G2}(x, y) & \text{for even } x, \text{ odd } y \text{ ("G2" type)} \\ f_B(x, y) & \text{for even } x, \text{ even } y \text{ ("B" type)}. \end{cases} \quad (\text{A7})$$

Using operators from secs. (1-3), $g(x, y)$ can be written as

$$\begin{aligned} g(x, y) = & \mathbf{T}_{(-1,-1)}\mathbf{U}_{(2,2)}\mathbf{D}_{(2,2)}\mathbf{T}_{(1,1)}f_R(x, y) + \\ & \mathbf{T}_{(-1,0)}\mathbf{U}_{(2,2)}\mathbf{D}_{(2,2)}\mathbf{T}_{(1,0)}f_{G1}(x, y) + \\ & \mathbf{T}_{(0,-1)}\mathbf{U}_{(2,2)}\mathbf{D}_{(2,2)}\mathbf{T}_{(0,1)}f_{G2}(x, y) + \\ & \mathbf{U}_{(2,2)}\mathbf{D}_{(2,2)}f_B(x, y) . \end{aligned} \quad (\text{A8})$$

For clarity, Fig. 17 illustrates in stages, the operations which are performed on $f_R(x, y)$, as written in the first row of Eq. (A8). In similar way, it follows that indeed Eqs. (A7,A8) are equivalent. We use the DTFT relations

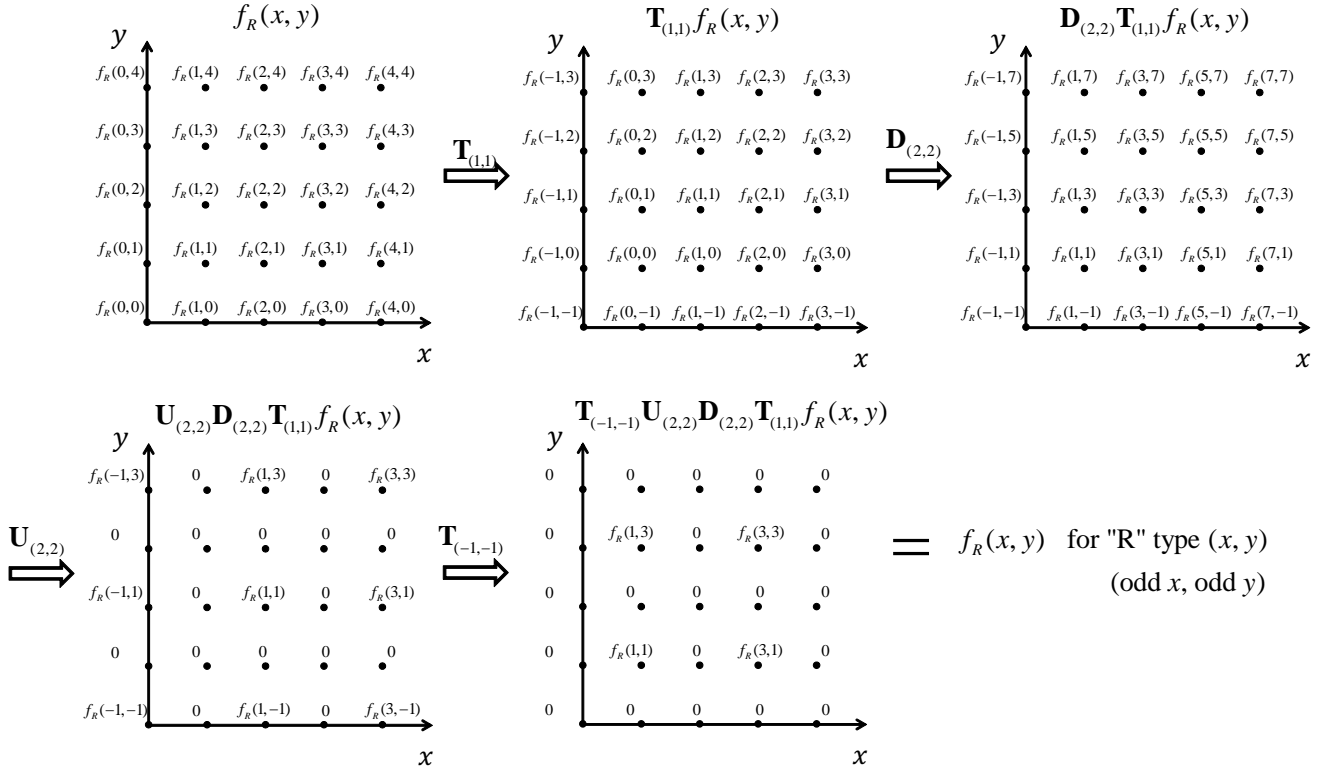


Fig. 17. A graphical illustration of the expression $\mathbf{T}_{(-1,-1)} \mathbf{U}_{(2,2)} \mathbf{D}_{(2,2)} \mathbf{T}_{(1,1)} f_R(x, y)$.

in secs. (1-3), and the notation in Eq. (4) to obtain the DTFT of Eq. (A8)

$$\begin{aligned}
 G(u, v) = & \frac{1}{4} \left[\tilde{f}_R - \tilde{f}_R^\uparrow - \tilde{f}_R^\rightarrow + \tilde{f}_R^\nearrow \right] + \\
 & \frac{1}{4} \left[\tilde{f}_{G1} + \tilde{f}_{G1}^\uparrow - \tilde{f}_{G1}^\rightarrow - \tilde{f}_{G1}^\nearrow \right] + \\
 & \frac{1}{4} \left[\tilde{f}_{G2} - \tilde{f}_{G2}^\uparrow + \tilde{f}_{G2}^\rightarrow - \tilde{f}_{G2}^\nearrow \right] + \\
 & \frac{1}{4} \left[\tilde{f}_B + \tilde{f}_B^\uparrow + \tilde{f}_B^\rightarrow + \tilde{f}_B^\nearrow \right]. \quad (\text{A9})
 \end{aligned}$$

Eqs. (5,10) follow this relation.

Appendix B: Proof of Eq. (13)

Applying Eq. (7) into Eq. (10), we obtain

$$\begin{aligned}
 S_c^{\text{int}}(u, v) = & \tilde{S}_c C_1 + \tilde{S}_c^\uparrow C_2 + \tilde{S}_c^\rightarrow C_3 + \tilde{S}_c^\nearrow C_4 + \\
 & S_c(u, v-1) C_5 + S_c(u-1, v) C_6 + \\
 & S_c\left(u - \frac{1}{2}, v-1\right) C_7 + S_c\left(u-1, v - \frac{1}{2}\right) C_8 + \\
 & S_c(u-1, v-1) C_9, \quad (\text{B1})
 \end{aligned}$$

where

$$\begin{aligned}
 C_1 &= \text{VMTF}_c^{\text{samp}} \cdot \text{VMTF}_c^{\text{int}} \\
 C_2 &= \left[\text{SR}_{c,\uparrow}^{\text{samp}} \cdot \text{VMTF}_c^{\text{int}} + \text{VMTF}_c^{\text{samp}} \cdot \text{SR}_{c,\uparrow}^{\text{int}} \right] \\
 C_3 &= \left[\text{SR}_{c,\rightarrow}^{\text{samp}} \cdot \text{VMTF}_c^{\text{int}} + \text{VMTF}_c^{\text{samp}} \cdot \text{SR}_{c,\rightarrow}^{\text{int}} \right] \\
 C_4 &= \left[\text{SR}_{c,\nearrow}^{\text{samp}} \cdot \text{VMTF}_c^{\text{int}} + \text{SR}_{c,\rightarrow}^{\text{samp}} \cdot \text{SR}_{c,\uparrow}^{\text{int}} + \right. \\
 & \quad \left. \text{SR}_{c,\uparrow}^{\text{samp}} \cdot \text{SR}_{c,\rightarrow}^{\text{int}} + \text{VMTF}_c^{\text{samp}} \cdot \text{SR}_{c,\nearrow}^{\text{int}} \right] \quad (\text{B2}) \\
 C_5 &= \text{SR}_{c,\uparrow}^{\text{samp}} \cdot \text{SR}_{c,\uparrow}^{\text{int}} \\
 C_6 &= \text{SR}_{c,\rightarrow}^{\text{samp}} \cdot \text{SR}_{c,\rightarrow}^{\text{int}} \\
 C_7 &= \left[\text{SR}_{c,\nearrow}^{\text{samp}} \cdot \text{SR}_{c,\uparrow}^{\text{int}} + \text{SR}_{c,\uparrow}^{\text{samp}} \cdot \text{SR}_{c,\nearrow}^{\text{int}} \right] \\
 C_8 &= \left[\text{SR}_{c,\nearrow}^{\text{samp}} \cdot \text{SR}_{c,\rightarrow}^{\text{int}} + \text{SR}_{c,\rightarrow}^{\text{samp}} \cdot \text{SR}_{c,\nearrow}^{\text{int}} \right] \\
 C_9 &= \text{SR}_{c,\nearrow}^{\text{samp}} \cdot \text{SR}_{c,\nearrow}^{\text{int}}.
 \end{aligned}$$

Fig. 18 is a visual representation of Eq. (B1). The terms involving $S_c(u, v-1)$, $S_c(u-1, v)$, $S_c(u - \frac{1}{2}, v-1)$, $S_c(u-1, v - \frac{1}{2})$ and $S_c(u-1, v-1)$ are frequency components greater than the nyquist frequency, $(u_{\text{nyq}}, v_{\text{nyq}}) = (\frac{1}{2}, \frac{1}{2})$. Therefore, they result in aliasing, and are reproduced at lower frequencies instead. Thus, Eq. (B1) becomes Eq. (13).

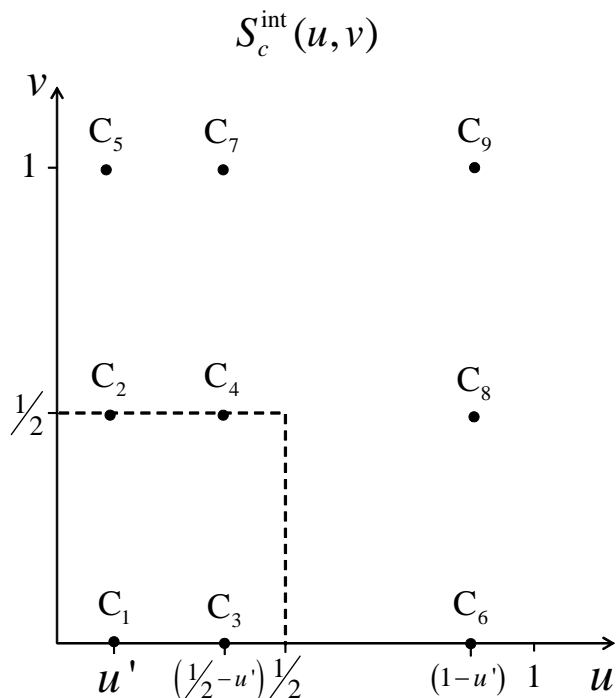


Fig. 18. A visual representation of $S_c^{\text{int}}(u, v)$, according to Eq. (B1).

References

- [1] F. Yasuma, T. Mitsunaga, D. Iso, and S. K. Nayar. Generalized assorted pixel camera: postcapture control of resolution, dynamic range, and spectrum. *IEEE Trans. on Image Processing*, 19(9):2241–2253, 2010.
- [2] J. Couillaud, A. Horé, and D. Ziou. Nature-inspired color-filter array for enhancing the quality of images. *JOSA A*, 29(8):1580–1587, 2012.
- [3] B. E. Bayer. Color imaging array. *US Patent 3,971,065*.
- [4] H. S. Malvar, L.-W. He, and R. Cutler. High-quality linear interpolation for demosaicing of bayer-patterned color images. In *Proc. of IEEE ICASSP*, volume 3, pages iii–485, 2004.
- [5] R. Ramanath, W. E. Snyder, G. L. Bilbro, and W. A. Sander. Demosaicking methods for bayer color arrays. *SPIE Journal of Electronic Imaging*, 11(3):306–315, 2002.
- [6] B. K. Gunturk, J. Glotzbach, Y. Altunbasak, R. W. Schafer, and R. M. Mersereau. Demosaicking: color filter array interpolation. *Signal Processing Magazine, IEEE*, 22(1):44–54, 2005.
- [7] A. Lukin and D. Kubasov. High-quality algorithm for bayer pattern interpolation. *Programming and Computer Software*, 30(6):347–358, 2004.
- [8] D. D. Muresan, S. Luke, and T. W. Parks. Reconstruction of color images from ccd arrays. *Proc. of Texas Instruments Digital Signal Processing Systems Fest*, pages 1–6, 2000.
- [9] S. Bobrov and Y. Y. Schechner. Image-based prediction of imaging and vision performance. *JOSA A*, 24(7):1920–1929, 2007.
- [10] N. Kopeika. A system engineering approach to imaging. SPIE-International Society for Optical Engineering, 1998. chap. 9, 10, 19.
- [11] A. Gordon. Prediction and measurement of minimum resolvable contrast for tv sensors. In *Proc. SPIE*, pages 533–542, 1994.
- [12] E. Dubois. Frequency-domain methods for demosaicking of bayer-sampled color images. *IEEE SPL*, 12(12):847–850, 2005.
- [13] Y. Elor, E. Pinsky, and A. Yaacobi. MTF for Bayer pattern color detector. In *Proc. SPIE*, volume 6567, 2007.
- [14] P. M. Hubel, J. Liu, and R. J. Guttosch. Spatial frequency response of color image sensors: Bayer color filters and foveon x3. In *Proc. SPIE*, volume 5301, pages 402–407, 2004.
- [15] L. G. Shapiro. Object and concept recognition for content-based image retrieval. <http://www.cs.washington.edu/research/imagedatabase/>.
- [16] The University of British Columbia. Signals and Communications (EECE 359) Course Notes, chapter 5 - The Discrete-Time Fourier Transform. <http://courses.ece.ubc.ca/359/>.